Braz J Phys (2015) 45:138–146
DOI 10.1007/s13538-014-0274-y

SOCIEDADE BRASILEIRA DE FÍSICA

NUCLEAR PHYSICS

Study of Reaction Cross Section of Light Mass Nuclei Using Glauber Formalisms

Mahesh K. Sharma · R. N. Panda · Manoj K. Sharma · S. K. Patra

Received: 13 August 2014 / Revised: 25 September 2014 / Accepted: 2 October 2014 / Published online: 28 October 2014

Abstract We study the reaction dynamics of some light mass nuclei (Be-Ar isotopes). We use the well-known Glauber formalism with densities obtained from a recently developed simple effective interaction, in the frameword of the microscopic non-relativistic Hartree–Fock formalisms. For comparison, we used also densities from the relativistic mean field formalism. In general, the study of the reaction dynamics suggests that both formalisms reproduce well the experimental data, with a slight superiority of the relativistic mean field densities over those of non-relativistic Hartree–Fock. This is so for the majority of the chosen cases, except for a few nuclear halo systems.

Keywords Reaction cross section · Densities · Glauber model and RMF and non RMF models

M. K. Sharma · M. K. Sharma
School of Physics and Materials Science, Thapar University, Patiala, 147 004, Punjab, India

M. K. Sharma
e-mail: maheshphy82@gmail.com

M. K. Sharma
e-mail: msharma@thapar.edu

R. N. Panda (✉)
Department of Physics, ITER, Siksha O Anusandhan University, 751 030 Bhubaneswar, India
e-mail: rnpanda@iopb.res.in

S. K. Patra
Institute of Physics, Sachivalaya Marg, 751 005 Bhubaneswar, India
e-mail: patra@iopb.res.in

1 Introduction

The total reaction cross-section measurements at intermediate energy have been used extensively by the nuclear physics community to investigate the nuclear size and distribution of nucleons [1–17]. The advancement in radioactive ion beams (RIB) at intermediate energy made it possible to explore the nuclear chart, and it opened up new opportunities to investigate numerous exotic phenomena. The study of exotic nuclei, specially those around the drip-line, is of immense interest in present days [18–20]. Although, the drip line is well established at the doubly magic ^{24}O nucleus, the study of unbound oxygen isotopes [21] suggests the possibility of shifting the drip line. The observation regarding the existence of ^{40}Mg and ^{42}Al isotopes [22] beyond the drip line, given by various mass formulae, challenges the earlier predictions. Thus, the investigation of the drip line concept is a frontier topic in nuclear physics. The measurements of neutron separation energies and interaction cross sections for $p-sd$ and sd shell region suggest the existence of a new magic number N=16 [23], which is also supported by Hoffman et al. [24]. A recent ion beam measurement at RIKEN [25] suggests new magic numbers at N=6, 16, 32, 34, and so on, with increasing proton-neutron imbalance, which breaks down the conventional ones. Apart from it, another exotic phenomenon is the investigation of neutron (proton) halo feature of some nuclei. The new member ^{31}Ne is included in the family of neutron halo [26–29]. The isotope ^{31}Ne, with N=21, breaks the shell closure structure, and lies at island of inversion (IOI) [30]. The investigation of nuclear systems at the IOI is carried out quite extensively in recent times. The study of quadrupole collectivity in the neutron-rich nuclei, with N=29 and 30, using intermediate energy Coulomb excitation, supports the existence of ^{47,48}Ar at the IOI.

Measurements of nuclear reaction cross sections for ^{19,20,22}C suggest that the drip line nucleus ^{22}C has a halo structure [31, 32]. The one and two neutron removal cross sections and the momentum distributions also support the halo behavior for ^{22}C. The nucleus ^{22}C has N = 16, which is a new magic number in neutron-rich nuclei [23, 33], and it has a Borromean halo structure (^{21}C is unstable). Direct mass measurements using the time of flight technique suggest that some other nuclei like ^{19}B, ^{29}F, and ^{34}Na are additional Borromean halo nuclei [34]. The successful study of reaction cross sections in the framework of Glauber model for halo nuclei [35] using the density of a recently proposed simple effective interaction (SEI-I) [36, 37] motivates us to see the reaction cross section σ_R for the low mass region using this approach. For comparison, we have used the well-known relativistic mean field (RMF) [38–42] densities using the NL3 and NL-SH parameter sets.

The paper is organized as follows: In Section 1, a brief introduction is given and Section 2 contains the description of Glauber model. The calculations and results are presented in Section 3. The predictability of HF(SEI-I) model to explore the different features of nuclei is included in this section. Finally, the summary and conclusions are outlined in Section 4.

2 Formalisms

The well-known Glauber approach [43–46] is used for the study of reaction dynamics in light mass region. This formalism is wildly used for reaction dynamics and improved for exotic nuclear systems [47, 48]. The theoretical formalism to study the reaction cross sections using the Glauber approach has been given by R. J. Glauber [5, 43, 44]. The nucleus–nucleus elastic scattering amplitude is written as

$$F(q) = \frac{\iota K}{2\pi}\int dbe^{\iota q.b}(1 - e^{\iota\chi(b)}). \tag{1}$$

At low energy, this model is modified in order to take care of finite range effects in the profile function and Coulomb modified trajectories. The effect of Coulomb interaction has been introduced in elastic scattering by considering both the projectile and target as a point charge. Due to long range of Coulomb potential screening, radius a is introduced to shield the charges at a large distances [44, 47]. So, elastic scattering amplitude including the Coulomb interaction is expressed as

$$F(q) = e^{\iota\chi_s}\{F_{coul}(q) + \frac{\iota K}{2\pi}\int dbe^{\iota q.b + 2\iota\eta\ln(Kb)}(1 - e^{\iota\chi(b)})\}, \tag{2}$$

with the Coulomb elastic scattering amplitude

$$F_{coul}(q) = \frac{-2\eta K}{q^2}exp\{-2\iota\eta\ln(\frac{q}{2K}) + 2\iota arg\Gamma(1 + \iota\eta)\}, \tag{3}$$

where K is the momentum of projectile and q is the momentum transferred from the projectile to the target. Here, $\eta = Z_P Z_T e^2/\hbar v$ is the Sommerfeld parameter, v is the incident velocity of the projectile, and $\chi_s = -2\eta\ln(2Ka)$ with a being a screening radius. The elastic differential cross section is given by

$$\frac{d\sigma}{d\Omega} = |F(q)|^2. \tag{4}$$

Where the elastic differential cross section is independent from the screening radius. The standard Glauber form for the total reaction cross sections is expressed as [43, 45]

$$\sigma_R = 2\pi\int_0^\infty b[1 - T(b)]db, \tag{5}$$

where 'T(b)' is the transparency function with impact parameter 'b'. The function T(b) is calculated by

$$T(b) = exp[-\sum_{i,j}\sigma_{ij}\int\overline{\rho_{tj}}(s)\overline{\rho_{pi}}(|\vec{b} - \vec{s}|)\vec{ds}]. \tag{6}$$

Here, the summation indices i, j run over proton and neutron and subscript 'p' and 't' refers to projectile and target, respectively. σ_{ij} is the experimental nucleon–nucleon reaction cross section which depends on the energy. The z-integrated densities are defined as

$$\overline{\rho}(\omega) = \int_{-\infty}^{\infty}\rho(\sqrt{w^2 + z^2})dz, \tag{7}$$

with $\omega^2 = x^2 + y^2$. Initially, Glauber model was designed for the high energy approximation. However, it was found to work reasonably well for both the nucleus–nucleus reaction and the differential elastic cross sections over a broad energy range [46, 49]. The modified transparency function T(b) is given by

$$T(b) = exp\left[-\int_p\int_t\sum_{i,j}[\Gamma_{ij}(\vec{b} - \vec{s} + \vec{t})]\overrightarrow{\rho_{pi}}(\vec{t})\overrightarrow{\rho_{tj}}(\vec{s})\vec{ds}\vec{dt}\right]. \tag{8}$$

The profile function Γ_{NN} for optical limit approximation is defined as

$$\Gamma_{NN} = \Gamma_{ij}(b_{eff}) = \frac{1 - \iota\alpha_{NN}}{2\pi\beta_{NN}^2}\sigma_{NN}exp(-\frac{b_{eff}^2}{2\beta_{NN}^2}), \tag{9}$$

for finite range and

$$\Gamma_{NN} = \Gamma_{ij}(b_{eff}) = \frac{1 - \iota\alpha_{NN}}{2}\sigma_{NN}\delta(b), \tag{10}$$

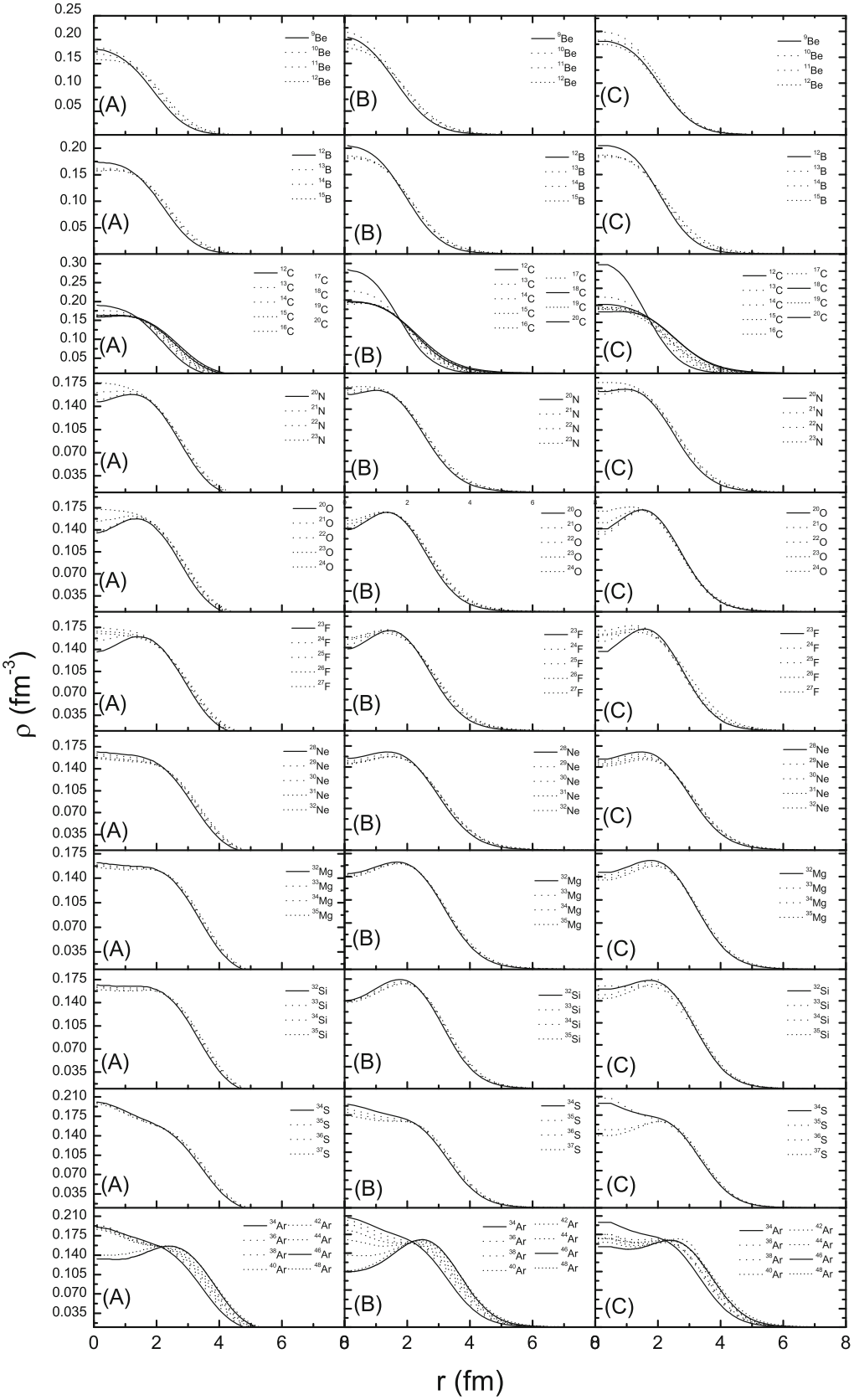

Fig. 1 Radial density plots for various isotopes of $^{9-12}$Be, $^{12-15}$B, $^{13-20}$C, $^{20-23}$N, $^{20-24}$O, $^{23-27}$F, $^{28-32}$Ne, $^{32-35}$Mg, $^{32-35}$Si, $^{34-37}$S, and $^{34-48}$Ar obtained by (*A*) HF(SEI-I), (*B*) Spherical RMF(NL3), and (*C*) Deformed RMF(NL3) formalism

for zero range with $b_{eff} = |\vec{b} - \vec{s} + \vec{t}|$, $\vec{b}$ is the impact parameter. Where $\vec{s}$ and $\vec{t}$ are the dummy variables for integration over the z-integrated target and projectile densities. The parameters σ_{NN}, α_{NN}, and β_{NN} usually depend upon the proton–proton, neutron–neutron, and proton–neutron interactions.

The study of reaction cross section by this approach strongly depends on the densities of the projectile and target nuclei. We use here the densities from axially deformed (Def.) as well as spherically (Sph.) symmetric RMF theory. As we have observed from our earlier calculations [50], the reaction cross section obtained from these densities is parameter dependent. Thus, we have used same set of NL3 parameter [51] in order to see the effect of deformations on reaction dynamics. The deformation effects are included in σ_R through the densities of projectile and target nuclei by taking axially deformed RMF(NL3) densities. The same set of reactions, studies have been carried by taking spherically symmetric RMF(NL3) densities for the sake of comparisons. We also compare the results obtained from both relativistic mean field and non-relativistic HF(SEI-I) densities.

3 Results and Discussions

The main ingredient of the Glauber model is the densities of projectile and target nuclei. Figure 1 represents the densities of the considered nuclei as a function of radial distance (r in fm). The nucleons distribution inside the nucleus is maximum at the center and starts decreasing continuously towards the surface. The left panel of the figure presents the nucleonic density distribution obtained by non-relativistic mean field HF(SEI-I) approach. The right panel shows spherical equivalent of deformed RMF densities with NL3 parameter. The central panel of the figure shows the density distribution obtained from spherical RMF model. It is clear from the figure that the densities of considered nuclei show similar kind of trend for all the formalism. A deep inspection on Fig. 1 indicates that some of the isotopes of O, F, Si, S, and Ar show depletion of the densities at the center, which is the primary indication for their bubble structure.

Figure 2 shows the quadrupole deformation parameter (β_2) of considered cases of nuclei obtained from RMF(NL3) formalism as a function of neutron number of respective isotopes. The negative β_2 values of nuclei in this figure signify oblate deformation, whereas positive values predict the prolate deformation and zero represents the spherical behavior. It is worthy to mention that the NL3 parameter set does not give a converged solution for many of the light nuclei as such. To get a converged result for such cases, we change the pairing strength

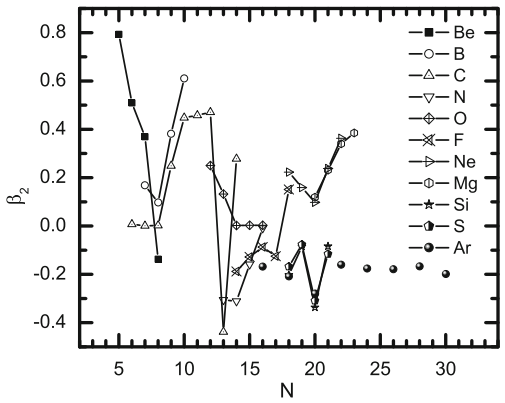

Fig. 2 The quadrupole deformation parameter β_2 for $^{9-12}$Be, $^{12-15}$B, $^{12-20}$C, $^{20-23}$N, $^{20-24}$O, $^{23-27}$F, $^{28-32}$Ne, $^{32-35}$Mg, $^{32-35}$Si, $^{34-37}$S, and $^{34-48}$Ar as a function of neutron number (N) for RMF(NL3)

$\triangle_{n,p}$ slightly in the BCS-pairing approach. As a result, we compromise a bit in the quadrupole deformation.

3.1 Total Reaction Cross Section

The densities from the well-known RMF with NL3 parameter are used from both axially deformed and spherically symmetric formalism along with the densities of HF(SEI-I). Our earlier work prompted us to see the effect of simple effective interaction on reaction dynamics for which one needs to fold these densities in terms of the Gaussian coefficients.

We have converted these densities of HF(SEI-I), Spherical, and deformed RMF(NL3) in term of Gaussian coefficients c_i and ranges a_i as

$$\rho(r) = \sum_{i=1}^{2} c_i exp[-a_i r^2]. \tag{11}$$

Another important ingredient for the evaluation of profile function in Glauber model is energy-dependent parameters σ_{NN}, α_{NN}, and β_{NN}, where σ_{NN} is the total nuclear reaction cross section in NN collision, α_{NN} is ratio of real to the imaginary part of forward nucleon-nucleon scattering amplitude, and β_{NN} is slope parameter, which determines the fall of the angular distribution of the NN scattering. These parameters are energy as well isospin dependent. Table 1 contains these energy-dependent parameters over energy range 30–1020 MeV/A. These parameters have been estimated by using the spline interpolation of values as suggested in Ref's. [52, 53].

To test the validity of the Glauber model, first of all we compared the reaction cross section σ_R obtained from the forces SEI-I, NL3, and NL-SH for ^{12}C+^{12}C with the

Table 1 The nucleon–nucleon cross section σ_{NN} and other parameters like α_{NN} and β_{NN} used to calculate the profile function [53]

E(MeV/A)	σ_{NN} (fm^2)	α_{NN}	β_{NN} (fm^2)
30.0	19.6	0.87	0.685
38.0	14.6	0.89	0.521
40.0	13.5	0.9	0.486
49.0	10.4	0.94	0.390
85.0	6.1	1.37	0.349
94.0	5.5	1.409	0.327
100.0	5.295	1.435	0.322
120.0	4.5	1.359	0.255
150.0	3.845	1.245	0.195
200.0	3.45	0.953	0.131
230.0	3.307790	0.7462136	0.1042526
240.0	3.266868	0.6800303	0.0978437
325.0	3.03	0.305	0.075
425.0	3.03	0.36	0.078
550.0	3.62	0.04	0.125
650.0	4.0	−0.095	0.16
730.0	4.174130	−0.0828693	0.1896611
740.0	4.189708	−0.0793203	0.1931483
760.0	4.217336	−0.0731153	0.1996571
790.0	4.250772	−0.0691061	0.2078210
800.0	4.26	−0.07	0.21
900.0	4.311690	−0.1439280	0.2171934
905.0	4.312775	−0.1498595	0.2170294
920.0	4.315433	−0.1684008	0.2163436
950.0	4.318554	−0.2078482	0.2142974
955.0	4.318853	−0.2146004	0.2138945
960.0	4.319103	−0.2213738	0.2134798
965.0	4.319310	−0.2281574	0.2130555
980.0	4.319725	−0.2484590	0.2117466
1000.0	4.32	−0.275	0.21
1005.0	4.320055	−0.2814692	0.2095773
1010.0	4.320110	−0.2878605	0.2091625
1020.0	4.320220	−0.3004108	0.2083566

experimental measurements in Fig. 3. It is clear from the figure that the calculated σ_R is quite sensitive to the density used. Even within the same interaction, it gives distinct results in the use of spherical or deformed densities. The theoretical results of Horiuchi et al. [53] are also given in the figure for comparison. Our spherical RMF(NL3) result matches well with the prediction of Ref. [53], but the deformed RMF(NL3) and spherical HF(SEI-I) overestimate the data.

Here, it is worthy to mention that the experimental quadrupole deformation parameter of ^{12}C is about 0.58, which we do not get by using NL3 or SEI parametrizations.

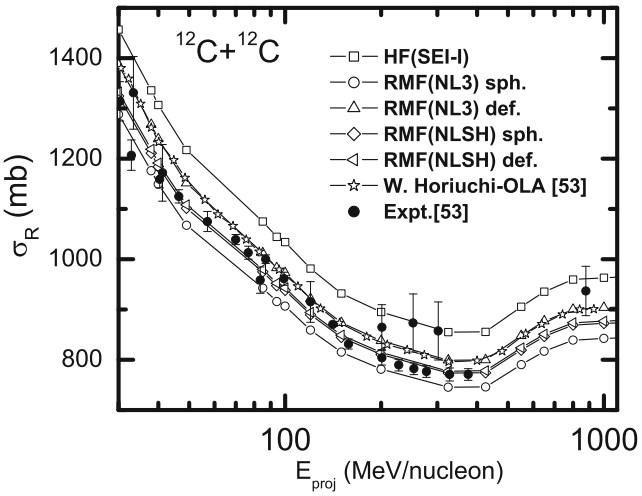

Fig. 3 The nuclear reaction cross section σ_R obtained from various densities for ^{12}C+^{12}C as a function of projectile energy. The available experimental data[53] are also given for comparison

We get $\beta_2 \sim -0.3$ in RMF(NL-SH) calculation. But the deformed solution of RMF(NL3) is slightly prolate, which may be the responsible factor for the deviation of RMF(NL3) results from the data. For low energy region, the data and prediction walk hand in hand confirming the applicability of the model. Again, for the evaluation of σ_R using Glauber model, both protons and neutrons density distributions are required as input. Thus, we cannot verify the model by using the experimental density as the neutrons density distribution does not available experimentally. Also, we are unable to reproduce the large prolate deformed solution of ^{12}C using any of the RMF forces and it is beyond the scope for the present SEI model for deformed calculations.

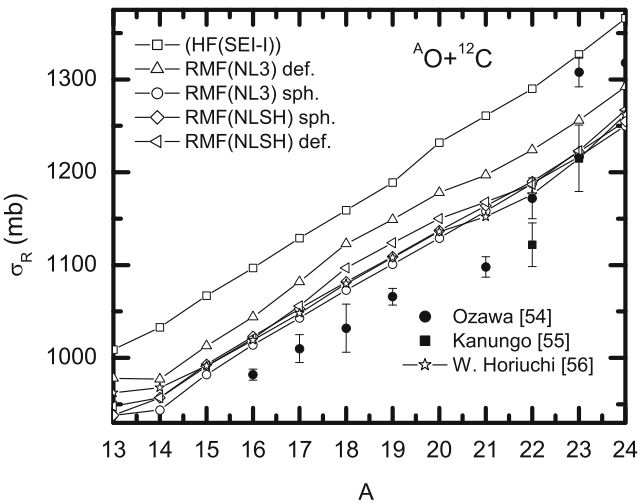

Fig. 4 The nuclear reaction cross section σ_R with various densities as a function of mass number for O-isotopes with ^{12}C target. The experimental data[54,55] and other predictions[56] are given for comparison

Table 2 The total nuclear reaction cross section (σ_R) and square of deviation (D_i) from experimental data (Expt.) for various projectiles with ^{12}C target using densities from HF(SEI), Sph RMF(NL3), and Def RMF(NL3). The experimental data [57–60] of reaction cross sections are also given for comparison

	Energy	σ_R (mb)				D_i^2		
Proj.	(MeV/A)	HF(SEI-I) (Sph.)	RMF(NL3) (Sph.)	RMF(NL3) (Def.)	Expt.	HF(SEI-I) (Sph.)	RMF(NL3) (Sph.)	RMF(NL3) (Def.)
^{9}Be	790	857	810	844	806±9	2601	16	1444
^{10}Be	790	894	836	860	813±10	6561	529	2209
^{11}Be	790	942	890	902	942±8	0	2704	1600
^{12}Be	790	986	894	1004	927±18	3481	1089	5929
^{12}B	790	972	875	909	866±7	11,236	81	1849
^{13}B	790	1012	916	960	883±14	16,641	1089	5929
^{14}B	790	1049	951	1029	929±26	14,400	484	10,000
^{15}B	790	1086	991	1080	962±160	15,376	841	13,924
^{13}C	960	1005	901	931	862±12	20,449	1521	4761
^{14}C	965	1003	944	978	880±19	15,129	4096	9604
^{15}C	730	1065	959	1026	945±10	14,400	196	6561
^{16}C	960	1113	1005	1084	1036±11	5929	961	2304
^{17}C	965	1147	1037	1117	1056±10	8281	361	3721
^{18}C	955	1182	1098	1150	1104±15	6084	36	2116
^{19}C	960	1215	1099	1120	1231±28	256	17,424	12,321
^{20}C	905	1271	1131	1179	1187±20	7056	3136	64
^{20}N	950	1239	1141	1174	1121±17	13,924	400	2809
^{21}N	1005	1270	1172	1195	1114±9	24,336	3364	6561
^{22}N	965	1306	1205	1278	1245±49	3721	1600	1089
^{23}N	920	1344	1240	1483	1399±98	3025	25,281	7056
^{20}O	950	1233	1130	1179	1078±10	24,025	2704	10,201
^{21}O	980	1261	1158	1197	1098±11	26,569	3600	9801
^{22}O	965	1291	1188	1225	1172±22	14,161	256	2809
^{23}O	960	1327	1218	1257	1308±16	361	8100	2601
^{24}O	965	1367	1251	1292	1318±52	2401	4489	676
^{23}F	1020	1316	1211	1250	1148±16	28,224	3969	10,404
^{24}F	1005	1354	1242	1299	1253±23	10,201	121	2116
^{25}F	1010	1393	1276	1363	1298±31	9025	484	4225
^{26}F	950	1434	1315	1388	1353±54	6561	1444	1225
^{28}Ne	240	1382	1272	1283	1273±11	11,881	1	100
^{29}Ne	240	1417	1302	1340	1344±14	5329	1764	16
^{28}Ne	950	1497	1378	1391	1244±40	64,009	17,956	21,609
^{29}Ne	950	1534	1410	1452	1279±32	65,025	17,161	29,929
^{30}Ne	240	1454	1339	1401	1348±17	11,236	81	2809
^{31}Ne	240	1481	1353	1408	1435±22	2116	6724	729
^{32}Ne	240	1509	1375	1417	1385±33	15,376	100	1024
^{32}Mg	900	1613	1482	1545	1331±24	79,524	22,801	45,796
^{32}Mg	950	1613	1482	1545	1340±24	74,529	20,164	42,025
^{33}Mg	900	1641	1505	1538	1320±23	103,041	34,225	47,524
^{34}Mg	900	1669	1526	1534	1372±46	88,209	23,716	26,244
^{35}Mg	900	1697	1548	1553	1472±70	50,625	5776	6561

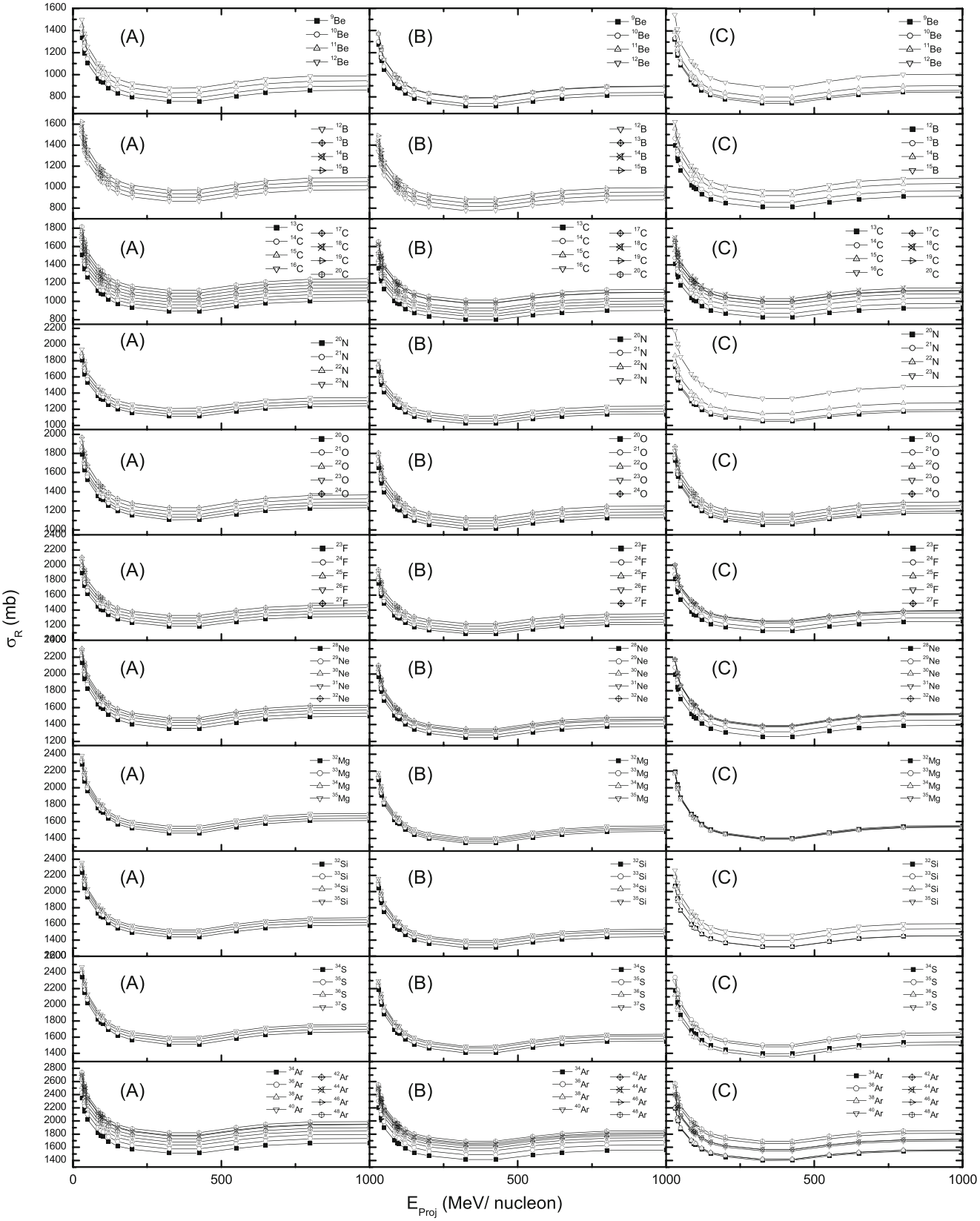

Fig. 5 Variation of total reaction cross-sections (σ_R) as a function of projectile energy (E_{proj}) using (**A**) HF(SEI-I), (**B**) Sph. RMF(NL3), (**C**) Def. RMF(NL3) densities for $^{9-12}$Be, $^{12-15}$B, $^{13-20}$C, $^{20-23}$N, $^{20-24}$O, $^{23-27}$F, $^{28-32}$Ne, $^{32-35}$Mg, $^{32-35}$Si, $^{34-37}$S and $^{34-48}$Ar nuclei. Here ^{12}C is used as target nucleus

Therefore, we may have an impression that these factors of densities cannot be overlooked while discussing the nuclear reaction cross section σ_R in Glauber model. The oblate shape of NL-SH parameter set for ^{12}C may be able to compensate in some sense of these limitations to reproduce the experimental data of σ_R.

The calculated results of σ_R for ^{A}O+^{12}C with various RMF and SEI-I densities are depicted in Fig. 4. For comparison, the recently measured experimental data [54, 55] along with other theoretical estimations [56] are also included. As far as the experimental data is concerned, the prediction of σ_R by Horiuchi et al. [56] and spherical RMF (both NL3 and NL-SH) almost agree with each other. Also, the reaction cross section obtained from the deformed NL-SH density agree well with the experimental estimations. Similar to the case of ^{12}C+^{12}C, unlike to the NL-SH predictions, the deformed NL3 results overestimate the data as shown in the figure. Here, also the same arguments may be hold good as it is discussed for ^{12}C+^{12}C to compare with the reaction cross section.

The calculated values of σ_R for the considered nuclei using the HF(SEI-I), spherical, and deformed RMF(NL3) densities are presented in the Table 2. The calculated reaction cross sections are also compared with the experimental data. One may clearly see from the table, that the σ_R obtained from both relativistic and non-relativistic formalism are well comparable with the experimental observation. We used the root mean square deviation or standard deviation (S.D) from experimental observation to analyse the best densities. The general expression of (S.D) can be defined as

$$S.D = \sqrt{\sum_{i=1}^{N} \frac{D_i^2}{N}} \tag{12}$$

$$D_i = (\sigma_R i(Obs) - \sigma_R i(Exp)). \tag{13}$$

The square of error of σ_R from experimental values are also presented in Table 2 for various densities. The values of $S.D$ for HF(SEI-I), spherical RMF(NL3), and deformed RMF(NL3) densities are 150.666, 78.584, and 97.438, respectively. The smallest value of $S.D$ for the spherical RMF(NL3) and deformed RMF(NL3) density suggests that the σ_R obtained with RMF density could reproduced better results as compared to the non-relativistic mean field densities. Where as σ_R values for ^{11}Be, ^{15}C, ^{19}C, ^{23}O, and ^{31}Ne (all considered halo nuclei) are 942, 1065, 1215, 1327, and 1481 mb with HF(SEI-I); 902, 1026, 1120, 1257, and 1408 mb with deformed RMF(NL3); 890, 959, 1099, 1218, and 1353 mb with spherical RMF(NL3) densities; and 942 $\pm$ 8, 945 $\pm$ 10, 1231 $\pm$ 28, 1308 $\pm$ 16, and 1435 $\pm$ 22 mb from the experimental data.

A deeper inspection to Table 2, one can easily interpret that the values of reaction cross sections obtained for particular halo systems and other exotic nuclei show better results with deformed RMF(NL3) and HF(SEI-I) densities. Figure 5 shows the total reaction cross sections of $^{9-12}$Be, $^{12-15}$B, $^{13-20}$C, $^{20-23}$N, $^{20-24}$O, $^{23-27}$F, $^{28-32}$Ne, $^{32-35}$Mg, $^{32-35}$Si, $^{34-37}$S, and $^{34-48}$Ar nuclei as a function of projectile energy (E_{proj}) over the energy range 30–1000 MeV/nucleon. The σ_R is higher at small E_{proj} and start decreasing up to the energy range of 300 MeV/nucleon. Small enhancement in σ_R is observed near 750 MeV/nucleon and after that it remains constant. The values of σ_R obtained from the HF(SEI-I) densities are slightly higher than the other densities (see Table 2). The reaction cross sections σ_R also increase by equal proportion in their isotopic chain with mass number A for both HF(SEI-I) and RMF(NL3) spherical densities. However, some disorderliness is recorded in the increase of σ_R for deformed RMF(NL3) densities. This effect may be due to the role of deformation in σ_R.

4 Summary and Conclusions

In summary, we have studied the structural properties and reaction cross sections of $^{9-12}$Be, $^{12-15}$B, $^{13-20}$C, $^{20-23}$N, $^{20-24}$O, $^{23-27}$F, $^{28-32}$Ne, $^{32-35}$Mg, $^{32-35}$Si, $^{34-37}$S, and $^{34-48}$Ar, in the framework of Glauber model. We used densities of non-relativistic Hartree–Fock calculations with a simple effective interaction and of the relativistic mean field formalism. In general, the σ_R obtained with RMF densities are better than those obtained with the non-relativistic HF(SEI-I) densities. This observation is in contrast with the remarkable success of SEI-I densities for halo nuclei. In a recent report [35], we have shown that the SEI-I densities reproduce the experimental nuclear reaction cross section for halo nuclei. In general, we observed that densities obtained from both formalisms can describe the nuclear reaction dynamics for most light nuclei. The RMF densities reproduce the data slightly better than the non-relativistic HF(SEI-I). Further use of these densities in various mass regions of the periodic table may impart better description of densities regarding the comparative analysis of these formalisms.

Acknowledgments Mahesh K. Sharma highly thankful to the institute of Physics, Bhubaneswar for their kind hospitality.

References

1. F.G. Brickwedde, J.R. Dunning, H.J. Hoge, J.H. Manley, Phys. Rev. **54**, 15 (1938)
2. H.A. Bethe, Phys. Rev. **57**, 15 (1940)
3. F.C. Nix, G.F. Clement, Phys. Rev **68**, 7 (1945)
4. K.M. Watson, Phys. Rev. **88**, 5 (1952)

5. R.J. Glauber, Phys. Rev. **100**, 1 (1955)
6. M.S. Hussein, R.A. Rego, C.A. Berrtulani, Phys. Rep. **201**, 279 (1991)
7. C.P. Swann, F.R. Metzer, Phys. Rev. **100**, 15 (1955)
8. W.L. Wong, R.G. Lipes, Phys. Rev. C **9**, 3 (1974)
9. J.S. Eck, J.R. Leigh, T.R. Ophel, P.D. Clark, Phys. Rev. C **21**, 6 (1980)
10. H.A. Khan, I.E. Qureshi, W. Westmeier, R. Brandt, P.A. Gottschalk, Phys. Rev. C **32**, 5 (1985)
11. I. Tanihata et al., Phys. Lett. B **287**, 307 (1992)
12. B. Abu-ibrahim, Y. Ogawa, Y. Suzuki, I. Tanihata, Comp. Phys. Commun. **151**, 369 (2003)
13. A. Shukla, B.K. Sharma, R. Chandra, P. Arumugam, S.K. Patra, Phys. Rev. C **76**, 034601 (2007)
14. S.K. Patra, R.N. Panda, P. Arumugam, R.K. Gupta, Phys. Rev. C **80**, 064602 (2009)
15. W. Horiuchi, Y. Suzuki, P. Capel, D. Baye, Phys. Rev. C **81**, 024606 (2010)
16. K. Minomo et al., Phys. Rev. Lett. **108**, 052503 (2012)
17. K. Wimmer et al., Phys. Rev. C **85**, 051603 (2012)
18. S.K. Patra, C.R. Praharaj, arXiv:1002.0654v1 [Nucl. th] (2010)
19. G. Saxena, D. Singh, Int. J. Mod. Phys. E **22**, 1350025 (2013)
20. S.K. Singh, S. Mahapatra, R.N. Mishra, Int. J. Mod. Phys. E **22**, 1350018 (2013)
21. C. Caesar et al., Phys. Rev. C **88**, 034313 (2013)
22. T. Baumann et al., Nature **449**, 1022 (2007)
23. A. Ozawa et al., Phys. Rev. Lett. **84**, 24 (2000)
24. C.R. Hoffman et al., Phys. Rev. Lett. **100**, 152502 (2008)
25. T. Otsuka et al., Phys. Rev. Lett. **87**, 082502 (2001)
26. I. Hamamoto, Phys. Rev. C **81**, 021304(R) (2010)
27. Y. Urata, K. Hagino, H. Sagawa, Phys. Rev. C **83**, 04130 (2011)
28. K. Minomo, T. Sumi, M. Kimura, K. Ogata, Y.R. Shimizu, M. Yahiro, Phys. Rev. C **84**, 034602 (2011)
29. M. Takechi et al., Phys. Lett. B **707**, 357 (2012)
30. E.K. Warburton et al., Phys. Rev. C **41**, 1147 (1990)
31. K. Tanaka et al., Phys. Rev. Lett. **104**, 062701 (2010)
32. N. Kobayshi et al., arXiv:1111.7196v1 [Nucl. ex] (2011)
33. I. Tanihata et al., Nucl. Phys. A **682**, 114c (2001)
34. L. Gaudefray et al., Phys. Rev. Lett **109**, 202503 (2012)
35. M.K. Sharma, S.K. Patra, Phys. Rev. C **87**, 044606 (2013)
36. B. Behera, X. Viñas, M. Bhuyan, T.R. Routray, B.K. Sharma, S.K. Patra, J. Phys. G: Nucl. Part. Phys. **40**, 095105 (2013)
37. T.R. Routray, X. Viñas, S.K. Tripathy, M. Bhuyan, S.K. Patra, B. Behera, J. Phys. Conf. Ser. **420**, 012114 (2013)
38. J. Boguta, A.R. Bodmer, Nucl. Phys. A **292**, 413 (1977)
39. W. Pannert, P. Ring, J. Boguta, Phys. Rev. Lett. **59**, 2420 (1987)
40. S.K. Patra, C.R. Praharaj, Phys. Rev. C **44**, 2552 (1991)
41. M. Del Estal, M. Centelles, X. Vinas, S.K. Patra, Phys. Rev. C **63**, 024314 (2001)
42. P. Ring, Prog. Part. Nucl. Phys. **37**, 193 (1996)
43. R.J. Glauber, Phys. Rev. **100**, 242 (1955)
44. R.J. Glauber, in ibid, Lectures on Theoretical Physics, ed. by W.E. Brittin, L.C. Dunham. Int. Sc., vol. 1 (New York, 1959), p. 315
45. P.J. Karol, Phys. Rev. C **11**, 1203 (1975)
46. J. Chauvin et al., Phys. Rev. C **28**, 1970 (1983)
47. B. Abu-Ibrahim et al., Nucl. Phys. A **657**, 391 (1999)
48. C.A. Bertulani, A. Gade, Comp. Phys. Comm. **175**, 372 (2006)
49. M. Buenerd et al., Nucl. Phys. A **424**, 313 (1948)
50. M.K. Sharma, M.S. Mehta, S.K. Patra, Int. J. Mod. Phys. E **22**, 135005 (2013)
51. G.A. Lalazissis, J. König, P. Ring, Phys. Rev. C **55**, 540 (1997)
52. L. Ray, Phys. Rev. C **20**, 1957 (1979)
53. W. Horiuchi, Y. Suzuki, B. Abu Ibrahim, A. Kohama, Phys. Rev. C **75**, 044607 (2007)
54. A. Ozawa et al., Nucl. Phys. A **693**, 32 (2001)
55. R. Kanungo et al., Phys. Rev. C **84**, 061304(R) (2011)
56. W. Horiuchi, T. Inakura, T. Nakatsukasa, Y. Suzuki, Phys. Rev. C **86**, 024614 (2012)
57. M. Fukuda et al., Phys. Lett. B **208**, 339 (1991)
58. T. Kobayashi et al., Phys. Lett. B **232**, 51 (1989)
59. I. Tanihata et al., Phys. Lett. B **206**, 592 (1988)
60. M. Takachi et al., Nucl. Phys. A **834**, 412c (2010)